Supplemental Information

Supplemental Figures and Legends

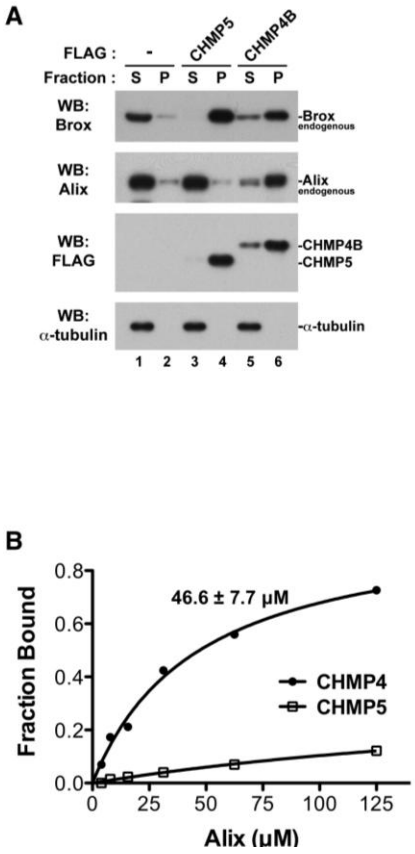

Figure S1, related to Figure 2: CHMP5 and CHMP4B have Different Specificity for Brox and Alix.

(A) CHMP5 overexpression induced the redistribution of endogenous Brox, but not Alix, to the detergent-resistant membrane fraction. HEK293T cells were transfected with either empty vector (lanes 1-2), FLAG-tagged CHMP5 (lanes 3-4) or CHMP4B (lanes 5-6). Forty-eight hours post transfection, cells were lysed and fractionated into soluble (S) and pellet (P) fractions as described in Material and Methods. Distribution of FLAG-tagged ESCRT-III and endogenous Brox and

Alix was analyzed by western blot using the indicated antibodies. α-tubulin was used as a control protein for the soluble fraction.

(B) The Alix Bro1 domain binds CHMP4B but not CHMP5. The Alix Bro1 domain binds CHMP4B with a dissociation constant of 46.6$\pm$7.7 μM similar to a previous report (McCullough et al., 2008), but its affinity for CHMP5 is negligible.

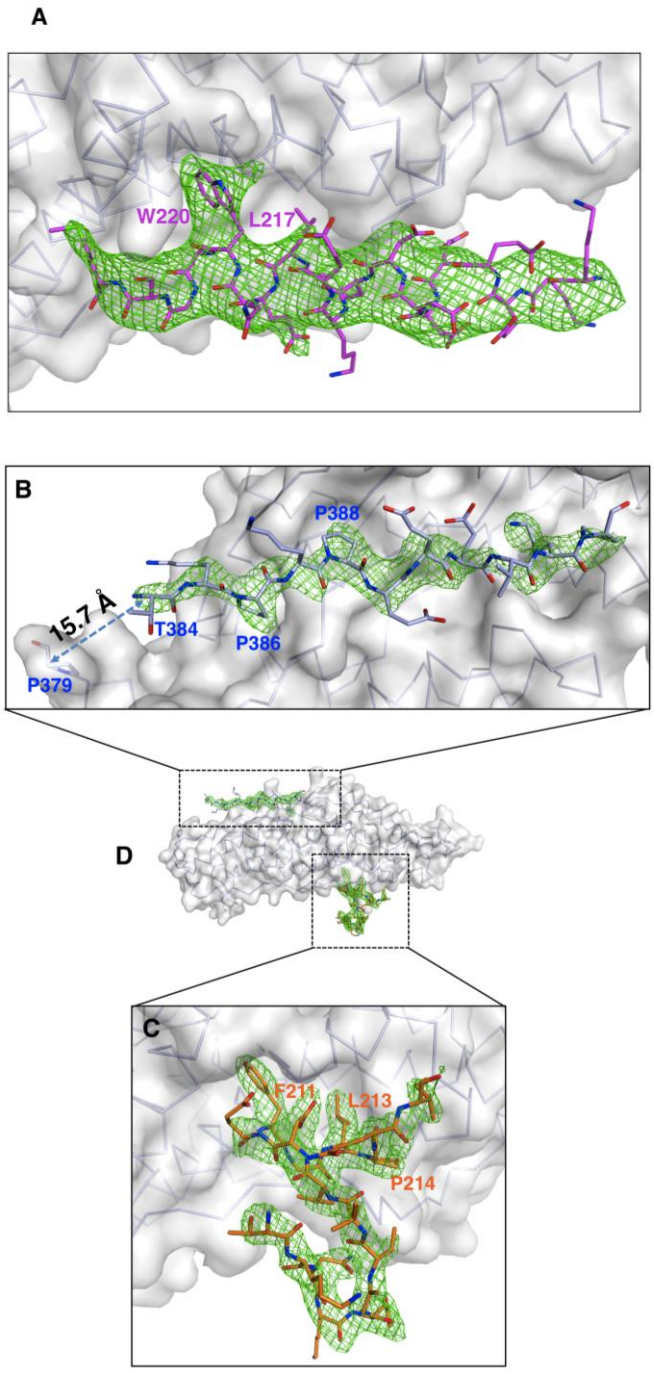

Figure S2, related to Figure 3: Electron density maps for the CHMP4B and CHMP5.

(A) The *Fo-Fc* omit map calculated at 3.8 Å resolution (contoured at 3 σ) for the CHMP4B C-terminal tail is shown as green mesh, with the refined CHMP4 residues shown in magenta.

(B) The *Fo-Fc* omit map calculated at 2.6 Å resolution (contoured at 3 σ) for the Brox residues T384-P394 is shown as green mesh, with the refined Brox residues shown in lightblue. The distance between Brox residues P379 and T384 is marked.

(C) The *Fo-Fc* omit map calculated at 2.6 Å resolution (contoured at 3 σ) for the CHMP5 C-terminal tail is shown as green mesh, with the refined CHMP5 residues shown in orange.

(D) An overview of the Brox:CHMP5 structure to show the general locations of (B) and (C).

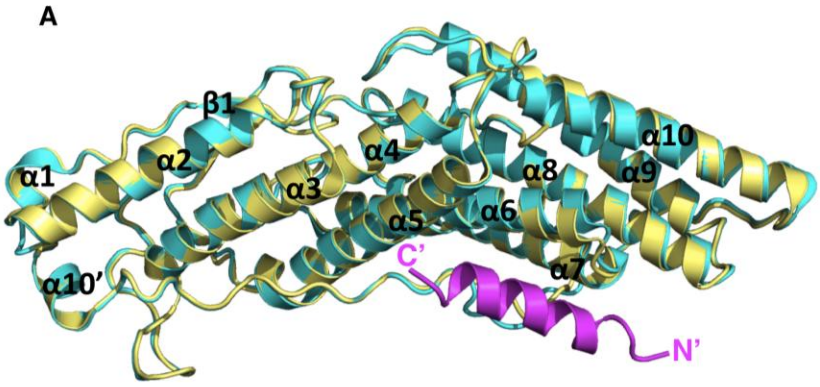
A
β1
α1
α2
α3
α4
α5
α6
α7
α8
α9
α10
α10'
C'
N'

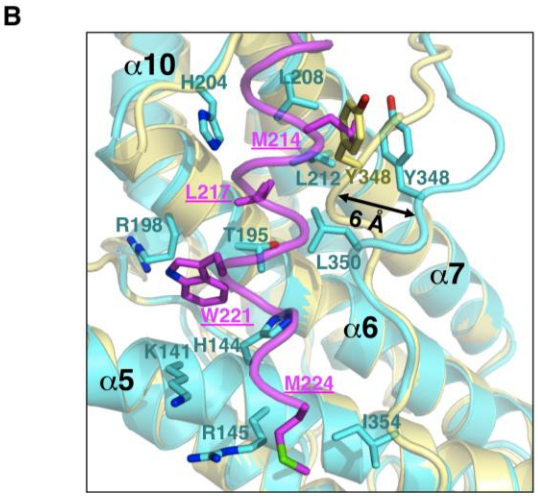
B
α10
H204
L208
M214
L212
Y348
Y348
L217
6 Å
R198
T195
L350
α7
W221
α6
K141
H144
α5
M224
R145
I354

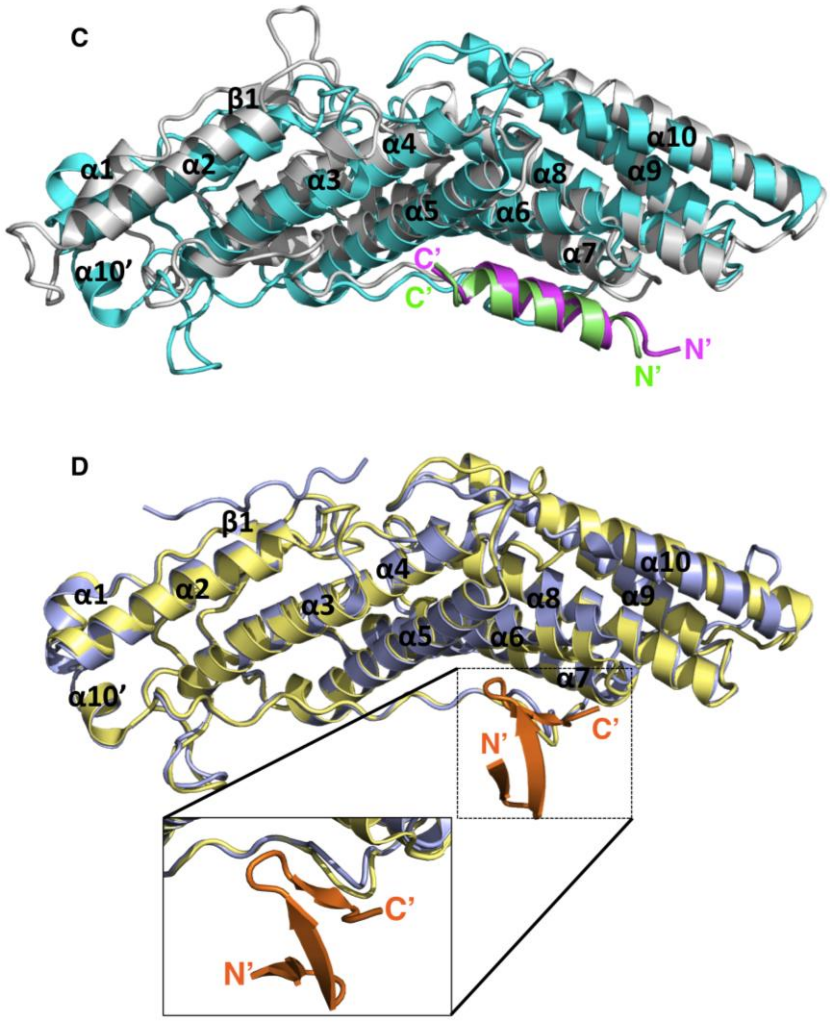

Figure S3, related to Figure 4: Comparison of the Bro1 domain structures in the presence and absence of CHMP4B or CHMP5.

(A) The Brox:CHMP4B structure is shown as cyan and magenta ribbons, respectively, and the Brox structure previously reported (3R9M) is superimposed and shown in yellow ribbons. Details of the Brox:CHMP4B interface denoted with a red circle is shown in (B).

(B) Details of the Brox:CHMP4B interface compared with the isolated Brox structure with the same color scheme as in (A). The view is similar to that in

Figure3B. A large shift in the Brox loop near residue Y348 is shown with a black arrow.

(C) The Brox:CHMP4B and Alix:CHMP4B (3C3Q) structures are superimposed and shown as cyan:magenta and gray:lime ribbons, respectively.

(D) The Brox:CHMP5 and Brox (3R9M) structures are superimposed and shown as lightblue:orange and yellow ribbons, respectively. A close-up view of the Brox C-terminal loop in contact with CHMP5 is shown at the lower panel.

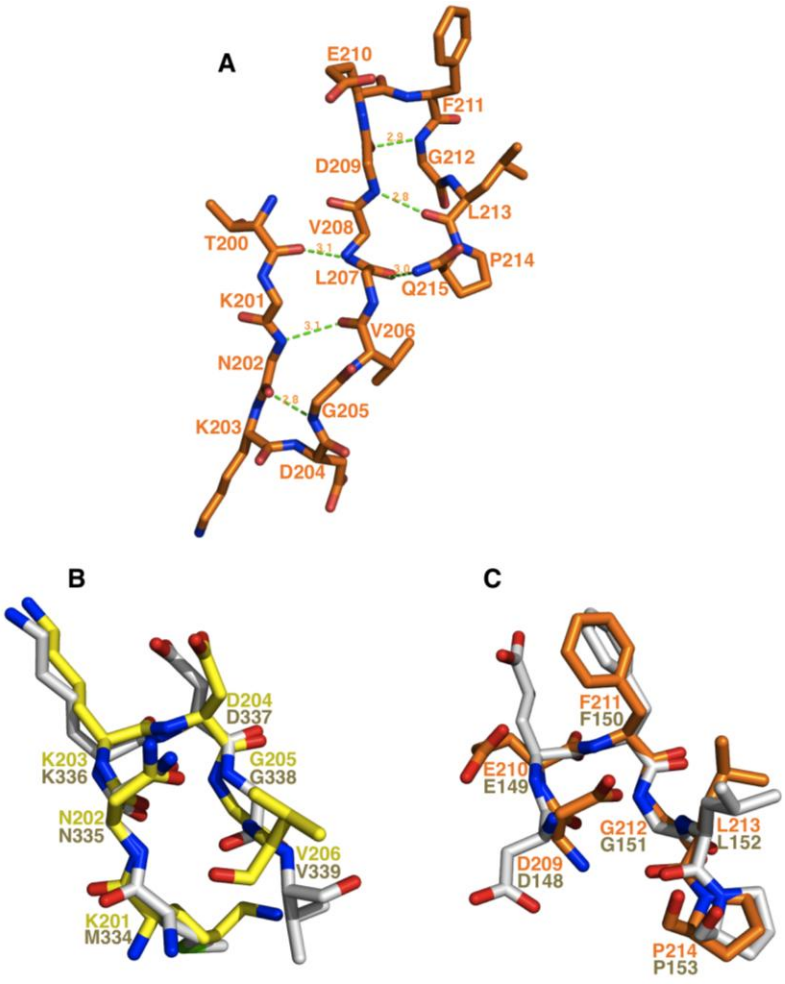
A
E210
F211
D209
G212
L213
V208
T200
P214
L207
Q215
K201
V206
N202
G205
K203
D204
B
D204
D337
K203
K336
G205
G338
N202
N335
V206
V339
K201
M334
C
F211
F150
E210
E149
G212
G151
L213
L152
D209
D148
P214
P153
CHMP5 201-206
1FM6 334-339
CHMP5 209-214
1F6Y 148-153

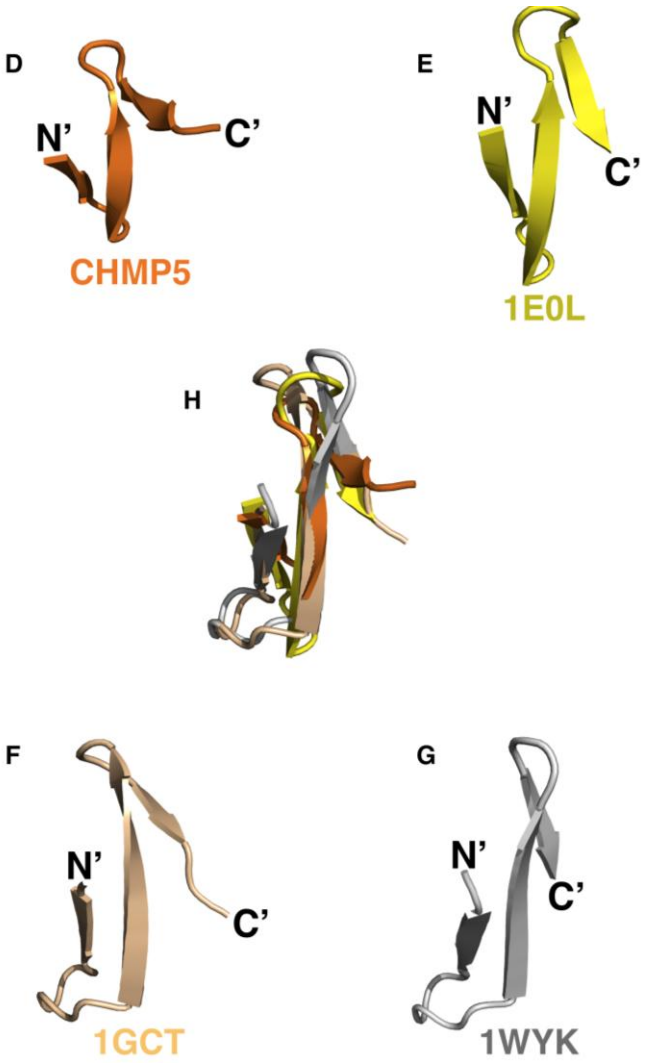

Figure S4, related to Figure 5: The tandem β-hairpin structure of the CHMP5 C-terminal tail.

(A) Schematic representation of the CHMP5 C-terminal tail as sticks. The main-chain hydrogen bonds are indicated as green dotted lines along with the bond distances. For clarity, the side-chains of K201, N202, L207, V208, D209 and Q215 are omitted. The main-chain torsion angles between residues L207 and V208 are adjusted from the crystal structure to demonstrate the overall tandem β-hairpin fold without changing the main-chain hydrogen bonding distances.

(B) Comparison of the CHMP5 first β-hairpin (yellow) with that from PPARgamma (1FM6, gray) with almost identical sequences.

(C) Comparison of the CHMP5 second β-hairpin (orange) with that from methyltransferase (1F6Y, gray) with identical sequences.

(D) The tandem β-hairpin structure from CHMP5 is shown in orange ribbons.

(E) The tandem β-hairpin structure from the WW domain of the formin binding protein (1E0L) is shown in yellow ribbons.

(F) The tandem β-hairpin structure from γ-chymotrypsin (1GCT) is shown in wheat ribbons.

(G) The tandem β-hairpin structure from the sindbis virus capsid protein (1WYK) is shown in gray ribbons.

(H) Superposition of (D-G) structures is shown.

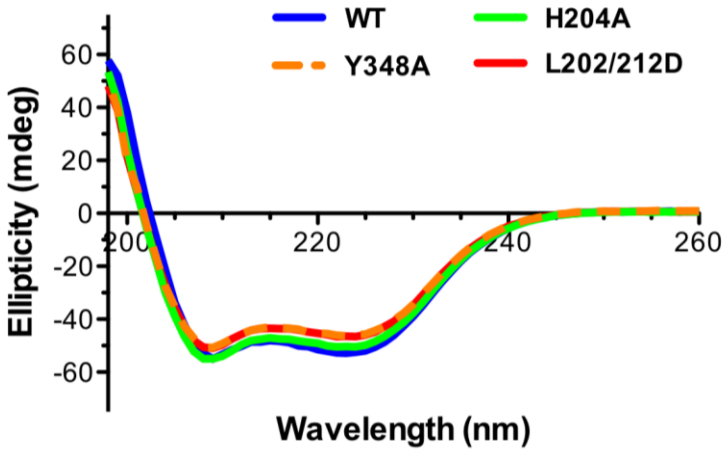

Figure S5, related to Figure 6: Mutation of The Brox Residues H204, Y348, L208 and L212 Do not Compromise Its Proper Folding.

The CD spectra of the wild type, H204A, Y348A, and L208/212D mutants of Brox were shown in blue, purple, green, and red, respectively.

Table S1. List of Peptides Used in the Fluorescence Polarization Assay (related to Table 1)

CHMP5	
WT	TKNKDGVLVDEFGLPQIPAS
F211A	TKNKDGVLVDE**A**GLPQIPAS
L213A	TKNKDGVLVDEFG**A**PQIPAS
P214G	TKNKDGVLVDEFGL**G**QIPAS

CHMP4B	
WT	KKKEEEDDDMKELENWAGSM
M214A	KKKEEEDDD**A**KELENWAGSM
L217A	KKKEEEDDDMKE**A**ENWAGSM
W220A	KKKEEEDDDMKELEN**A**AGSM

SUPPLEMTNAL EXPERIMENTAL PROCEDURES

Immunoprecipitation Assay.

The mammalian expression vectors for N-terminal HA-tagged human Alix, Brox, HD-PTP and Rhophilin-2 were reported previously (Dussupt et al., 2009). Expression vectors for ESCRT-III proteins were generated by PCR amplification from cDNA previously described (Dussupt et al., 2009) or purchased from Open Biosystems (Huntsville, AL) and subcloned into p3XFLAG-*myc*-CMV-26 (Sigma, St. Louis, MO). Point mutations were generated using the Quik-change mutagenesis kit (Stratagene, Santa Clara, CA). HEK293T cells were maintained in DMEM supplemented with 10% fetal bovine serum and transfected using Lipofectamine 2000 (Invitrogen, Carlsbad, CA) with the indicated expression vectors encoding HA- and FLAG-tagged proteins. Forty-eight hours post-transfection, the cells were harvested, washed in cold PBS and lysed in RIPA buffer (0.5 % Nonie P-40, 50 mM Hepes-Na pH 7.3, 150 mM NaCl, 2 mM EDTA, 20 mM β-glycerophosphate, 0.1 mM Na_3VO_4, 1 mM NaF, 1 mM PMSF, 0.5 mM DTT and complete protease inhibitor cocktail [Roche Applied Science, Indianapolis, IN]). The lysates were centrifuged at 16,100 × *g*, 4ºC, for 10 min and supernatants were incubated at 4ºC with agarose beads covalently linked to anti-HA mouse monoclonal antibody (Sigma, St. Louis, MO). The beads were then extensively washed in RIPA buffer prior to 2 successive elutions with HA peptide (100 mg/ml, Sigma, St. Louis, MO). Immunoprecipitates and cell lysates

(input fractions) were visualized by SDS-PAGE and western blot with anti-FLAG or anti-HA antibody (Sigma, St. Louis, MO).

Protein Expression and Purification.

The C-terminal fragments of human CHMP5 (residues 151-219) and human CHMP4B (residues 121-224) were cloned in a modified pET30a(+) vector (EMD Biosciences, San Diego, CA) between *NdeI* and *NotI* sites. The expressed proteins contained an N-terminal His6-tag followed by a cleavage site for the tobacco etch virus (TEV) protease. The expression vector were transformed into *E. coli* BL21 (DE3) cells and protein expression was induced with 0.5 mM isopropyl-β-d-thiogalactoside (IPTG) at OD_{600} = 0.6 and grew overnight at 15°C. Cells were harvested and lysed by sonication in a buffer containing 25 mM Tris-HCl, pH 8.0, 125 mM NaCl and 10 mM imidazole. Cleared cell lysates were purified by nickel affinity chromatography with a HisPrep FF 16/10 affinity column (GE Healthcare Biosciences, Piscataway, NJ) followed by TEV digestion at 4°C for 12 hr. The proteins were further purified by size-exclusion chromatography with a Superdex S200 column (GE Healthcare Biosciences, Piscataway, NJ) in a buffer containing 25 mM Tris-HCl pH 8.0 and 150 mM NaCl. A second nickel affinity chromatography was used to remove the His6-tagged TEV and digested expression tags. Two forms of human Brox proteins were used in this study: residues 2-411 and denoted “Broxl” in Table 1, and residues 2-377 and denoted “Broxs” in Table 1. The Brox and Alix Bro1 domains were expressed and purified

as reported previously (Sette et al., 2011) and similar to the above for the CHMP proteins. Both the “Broxl” and “Broxs” forms were used in co-crystallization with CHMP5, and only the “Broxl” form was used in co-crystallization with CHMP4B.

Structure Determination and Refinement.

Structures for the Brox:CHMP4B and Brox:CHMP5 complexes were determined by molecular replacement with program Phaser (McCoy, 2007) using the crystal structure of Brox (3R9M) (Sette et al., 2011) as a search model. Electron density maps calculated with the molecular replacement solutions showed clear positive densities at the concave surface of the Brox boomerang structure (Figure S2). The identity of the CHMP4B C-terminal tail was determined based on the prominent density for the CHMP4B W220 side-chain, the strong cylinder-shaped density for a helical structure, and the overall similarity between the Alix:CHMP4B (3C3Q) and Brox:CHMP4B structures (Figure S2A). The registry of the CHMP5 C-terminal tail was unambiguously determined based on the fact that electron density maps calculated with the CHMP5 C-terminal fragment (“-CHMP5”) and the 20 residue peptide (“-5C”) showed identical positive densities in this region, the prominent density for the F211 side-chain, no side-chain density for the adjacent G212, and the following LP sequence has a characteristic ring structure at the Proline main-chain (Figure S2C).

During structural determination of the Broxl-CHMP5 complex (Table 1), a second region of positive electron density was observed at the convex surface of

the Brox structure close to the last observed Bro1 domain residue P379 (Figure S2B). This density only appeared for crystals containing the “Broxl” form, irrespective of whether the 69 residue CHMP5 C-terminal fragment or the 20 residue peptide was used to obtain the crystals. We therefore reasoned that this density belonged to the Brox C-terminal region that was not included in the Bro1 domain model. Residues T384 to P394 were then built in the current model for the Broxl-CHMP5 and Broxl-5P structures based on the close proximity of the density to the last residue P379 of the Bro1 domain, and the characteristic bulged side chains of P386 and P388 in an extended Brox C-terminal region. Of note, the Cα atoms of P379 and T384 are separated by a distance of 15.7 Å, which would be consistent with an extended loop structure for the four unmodeled residues in between. Nonetheless, the current resolution does not allow for unambiguous determination of the amino acid side chains, and thus we can not formally exclude the possibility of alternative models. The Brox:CHMP5 structural models were built and refined using programs COOT (Emsley and Cowtan, 2004) and PHENIX (Adams et al., 2010), respectively. Analysis of the Brox:CHMP5 complex was performed based on the “Broxl-CHMP5” structure (Table 1) because of its higher resolution. The Brox:CHMP4 structure was refined with the deformable elastic network (DEN) approach incorporated in program CNS (Brünger et al., 1998; Schroder et al., 2010) using the 1.95 Å resolution crystal structure of Brox (3R9M) as a reference. Calculation of the solvent accessible surface area was carried out using program areaimol from the

CCP4 program suite (Lee and Richards, 1971; Potterton et al., 2003). All structure figures were prepared with program Pymol (Schrödinger, LLC.).

Supplemental References

Adams, P.D., Afonine, P.V., Bunkoczi, G., Chen, V.B., Davis, I.W., Echols, N., Headd, J.J., Hung, L.W., Kapral, G.J., Grosse-Kunstleve, R.W.*, et al.* (2010). PHENIX: a comprehensive Python-based system for macromolecular structure solution. Acta Crystallogr D Biol Crystallogr *66*, 213-221.

Brünger, A.T., Adams, P.D., Clore, G.M., Gros, P., Grosse-Kunstleve, R.W., Jiang, J.-S., Kuszewski, J., Nilges, M., Pannu, N.S., Read, R.J.*, et al.* (1998). Crystallography and NMR system (CNS): A new software suite for macromolecular structure determination. Acta Cryst. *D54*, 905-921.

Dussupt, V., Javid, M.P., Abou-Jaoude, G., Jadwin, J.A., de La Cruz, J., Nagashima, K., and Bouamr, F. (2009). The nucleocapsid region of HIV-1 Gag cooperates with the PTAP and LYPXnL late domains to recruit the cellular machinery necessary for viral budding. PLoS Pathog *5*, e1000339.

Emsley, P., and Cowtan, K. (2004). Coot: model-building tools for molecular graphics. Acta Crystallogr D Biol Crystallogr *60*, 2126-2132.

Lee, B., and Richards, F.M. (1971). The interpretation of protein structures: estimation of static accessibility. J. Mol. Biol. *55*, 379-400.

McCoy, A.J. (2007). Solving structures of protein complexes by molecular replacement with Phaser. Acta Crystallogr D Biol Crystallogr *63*, 32-41.

Potterton, E., Briggs, P., Turkenburg, M., and Dodson, E. (2003). A graphical user interface to the CCP4 program suite. Acta Crystallogr D Biol Crystallogr *59*, 1131-1137.

Schroder, G.F., Levitt, M., and Brunger, A.T. (2010). Super-resolution biomolecular crystallography with low-resolution data. Nature *464*, 1218-1222.

Sette, P., Mu, R., Dussupt, V., Jiang, J., Snyder, G., Smith, P., Xiao, T.S., and Bouamr, F. (2011). The Phe105 Loop of Alix Bro1 Domain Plays a Key Role in HIV-1 Release. Structure *19*, 1485-1495.